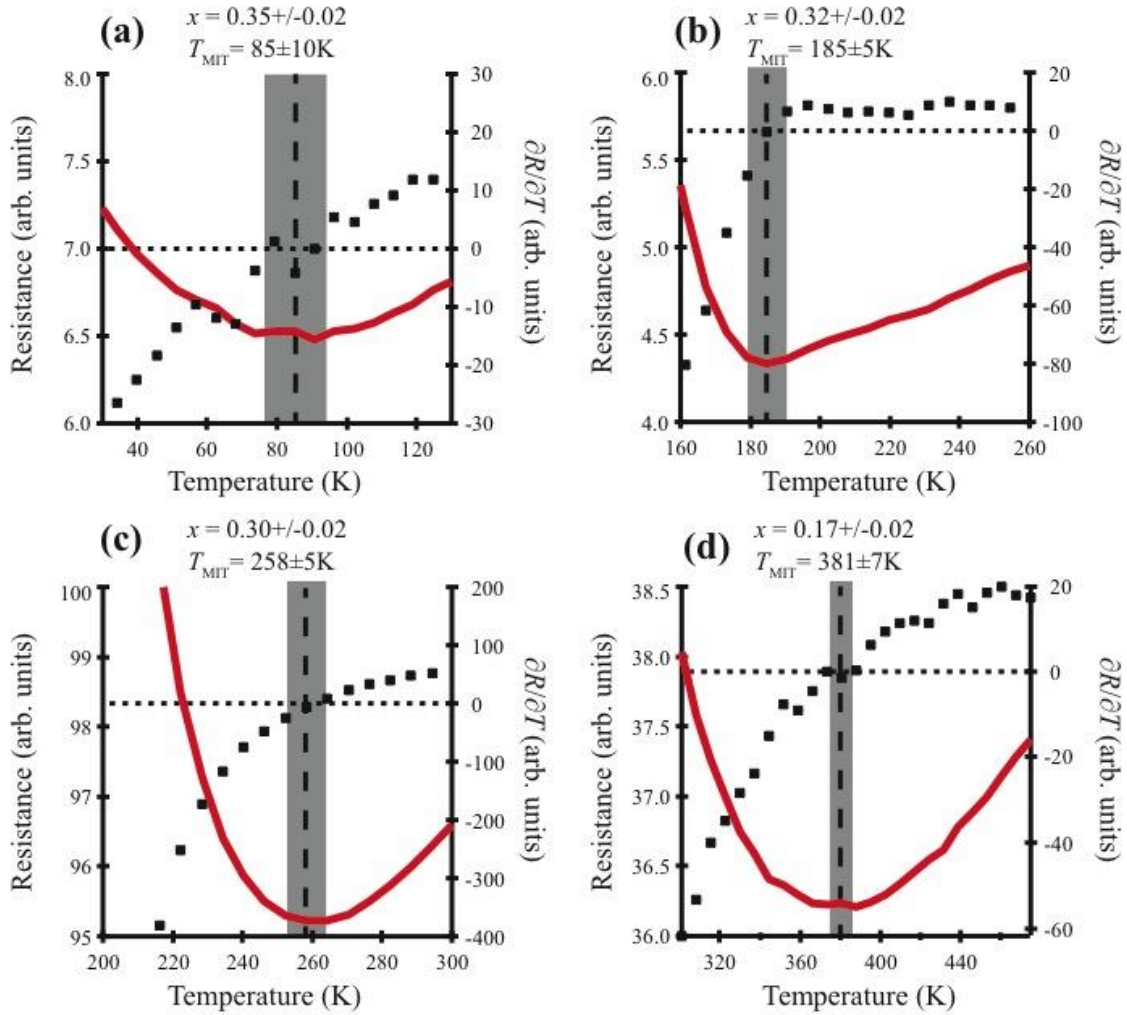
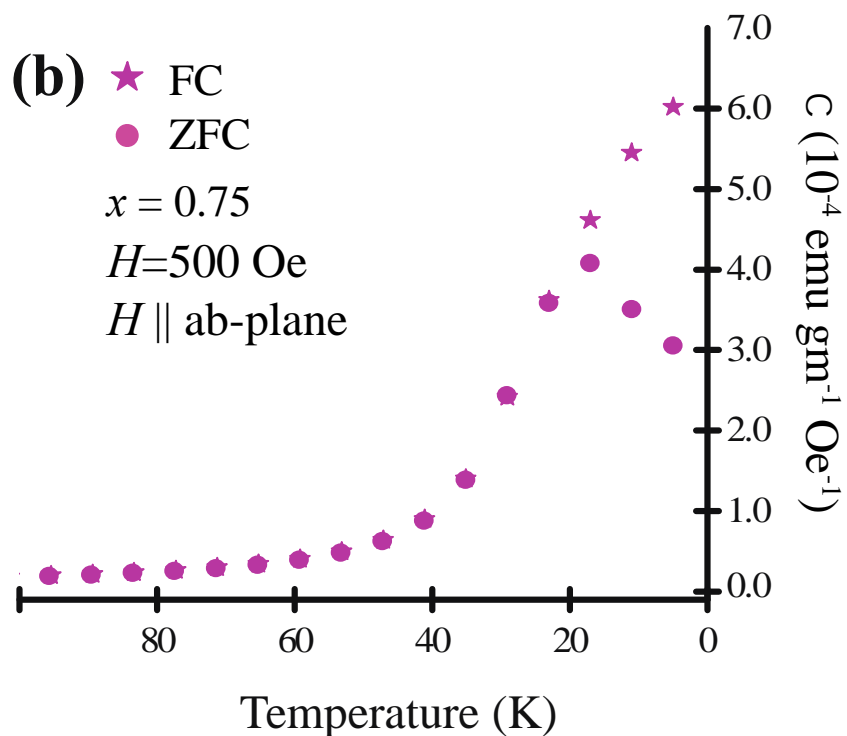
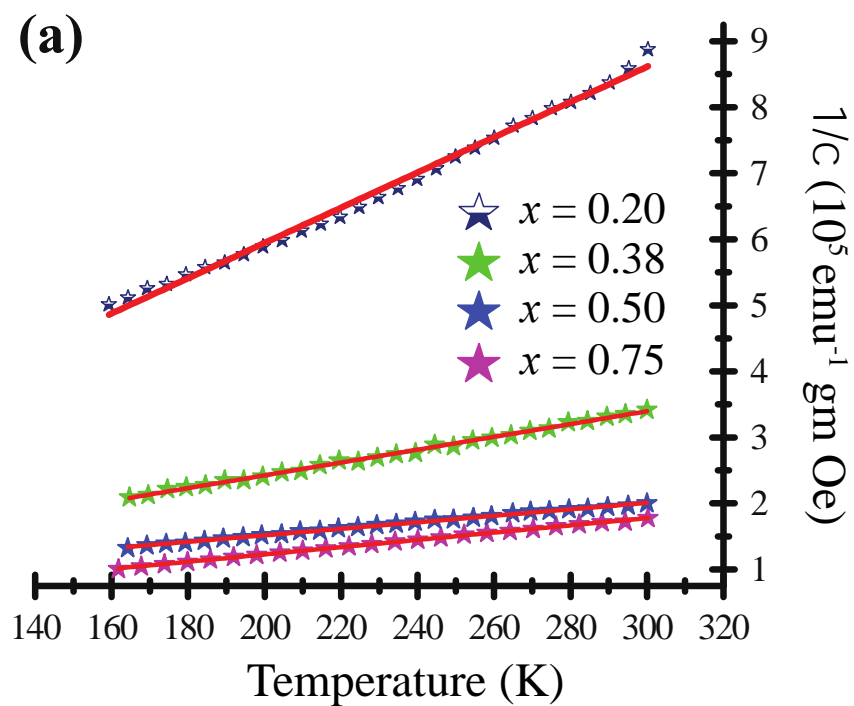


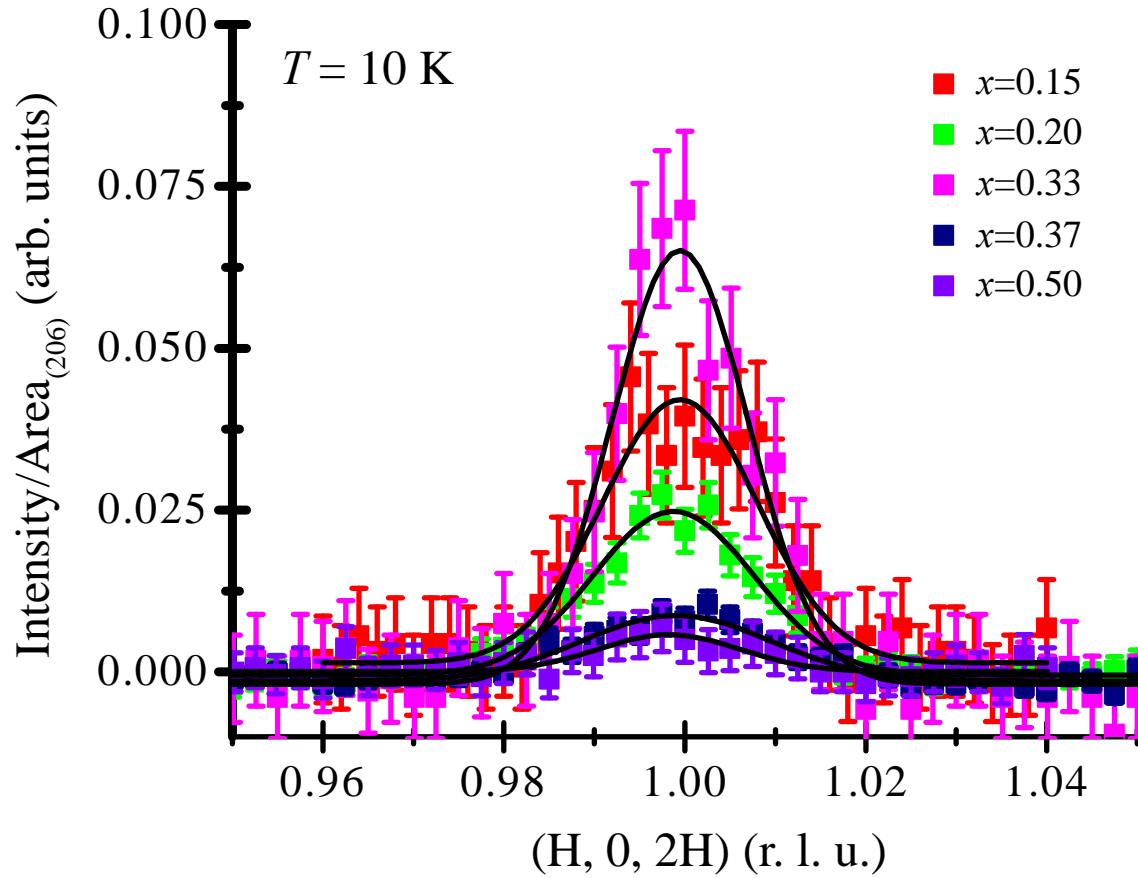
Supplementary Figures:



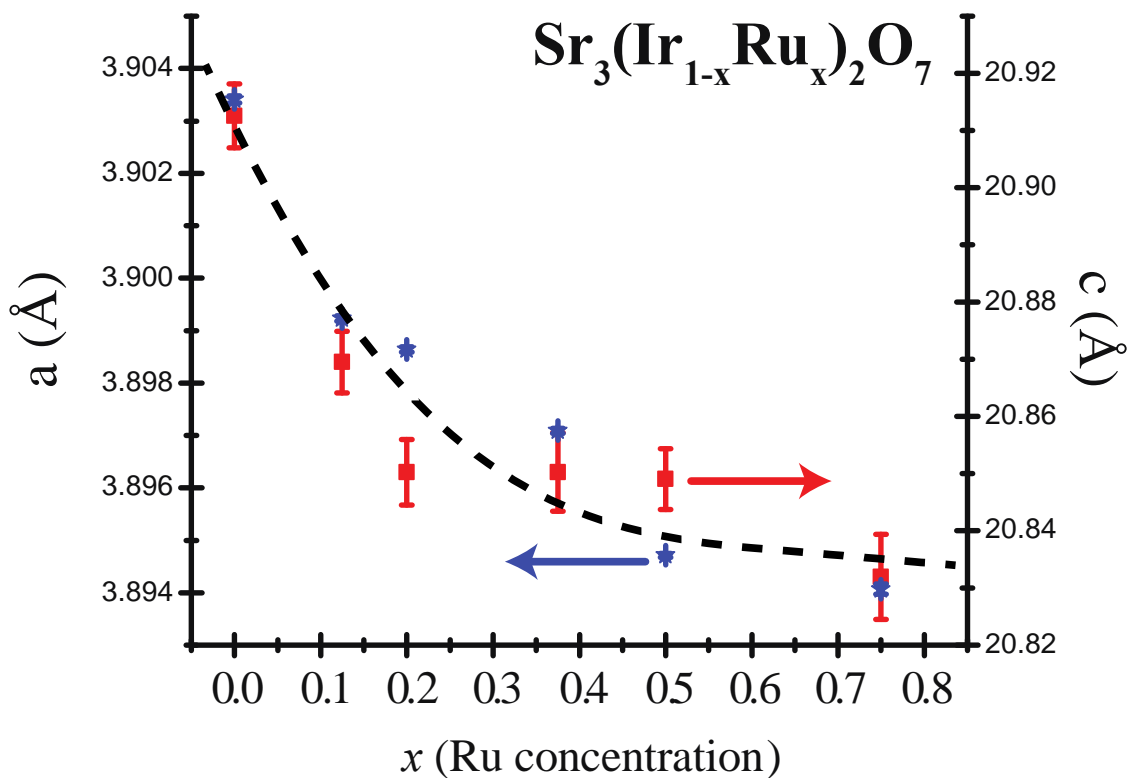
Supplementary Figure 1: Resistance (red lines) and its first derivative $\delta R/\delta T$ plotted (black squares) plotted as a function of temperature for $\text{Sr}_3(\text{Ir}_{1-x}\text{Ru}_x)_2\text{O}_7$ samples with (a) $x=0.35$, (b) $x=0.32$, (c) $x=0.3$, and (d) $x=0.17$ respectively. Vertical dashed lines show the temperature T_{MIT} plotted in the electronic phase diagram of Fig. 1 (a) in the paper's main text. Shaded grey region shows the uncertainty in determining T_{MIT} . Ru x-concentrations were measured for each sample with the corresponding uncertainty displayed in each panel. Resistance and $\delta R/\delta T$ are plotted as raw data in arbitrary units without geometric conversion to resistivity.



Supplementary Figure 2: (a) χ^{-1} as a function plotted as a function of temperature. A 500 Oe field was applied parallel to the ab-plane for all concentrations with the exception of $x=0.2$ where a 1 T field was applied. Solid lines are fits to Curie-Weiss behavior. (b) Zero-field cooled (ZFC) and field cooled (FC) magnetization data collected for the $x=0.75$ concentration. $1 \text{ emu g}^{-1} \text{ Oe}^{-1} = 4\pi \times 10^{-3} \text{ m}^3/\text{kg}$.



Supplementary Figure 3: Radial scans through the antiferromagnetic Bragg reflection $\mathbf{Q}=(1,0,2)$ for select concentrations of $\text{Sr}_3(\text{Ir}_{1-x}\text{Ru}_x)_2\text{O}_7$. Intensity for each sample has been divided by the integrated area of the sample's corresponding $\mathbf{Q}=(2,0,6)$ nuclear Bragg reflection. Before correcting for minor changes in absorption and extinction between Ru-concentrations this plot provides a rough illustration of the moment evolution as a function of x . Solid lines are Gaussian fits to the data. Error bars are one standard deviation. An additional sample, not plotted here, with nominal $x=0.32$ was measured with a normalized scattering intensity that saturates at 0.3 (off the scale) and the corresponding AF moment plotted in Fig. 3 (c) of the main text.



Supplementary Figure 4: Lattice parameters determined via powder x-ray diffraction on crushed crystals plotted as a function of Ru-doping for $\text{Sr}_3(\text{Ir}_{1-x}\text{Ru}_x)_2\text{O}_7$ at 300K. Data was refined using the FullProf Rietveld refinement program¹. Dashed line is a guide to the eye. While the reduction in lattice constants is monotonic, it is not linear and seemingly maps the nonlinear contraction previously observed in $\text{Sr}_2(\text{Ir}_{1-x}\text{Ru}_x)\text{O}_4$.² Error bars are one standard deviation.

Supplementary References:

¹ J. Rodriguez-Carvajal, Recent Advances in Magnetic Structure Determination by Neutron Powder Diffraction, *Physica B* 192, 55 (1993).

² R. J. Cava, B. Batlogg, K. Kiyono, H. Takagi, J. J. Krajewski, W. F. Peck, Jr., L. W. Rupp, Jr., and C. H. Chen, Localized-to-itinerant electron transition in $\text{Sr}_2\text{Ir}_{1-x}\text{Ru}_x\text{O}_4$, *Phys. Rev. B* 49, 11890 (1994).